



# Interannual to decadal variability of the Kuroshio extension: analyzing an ensemble of global hindcasts from a dynamical system viewpoint

Giusy Fedele<sup>1,2</sup> · Thierry Penduff<sup>3</sup> · Stefano Pierini<sup>4</sup> · M. Carmen Alvarez-Castro<sup>5,6</sup> · Alessio Bellucci<sup>5,7</sup> · Simona Masina<sup>2</sup>

Received: 8 April 2020 / Accepted: 26 March 2021 / Published online: 20 April 2021  
© The Author(s), under exclusive licence to Springer-Verlag GmbH Germany, part of Springer Nature 2021

## Abstract

The Kuroshio Extension (KE) is the inertial meandering jet formed by the convergence of the Kuroshio and Oyashio currents in the Northern Pacific. It is widely mentioned in the literature that the KE variability is bimodal on interannual to decadal time scale. The nature of this low frequency variability (LFV) is still under debate; intrinsic oceanic mechanisms are known to play a fundamental role in the phenomenon but there is also evidence from observations that the KE LFV is connected with changes in broader patterns associated with the Pacific Decadal Oscillation, which is in its turn generated by the dominant decadal mode of the sea level pressure variability in the North Pacific. We investigate the respective contributions of oceanic and atmospheric drivers of the KE variability by taking advantage of the OCCIPUT 1/4° global model dataset: it consists in an ensemble of 50 ocean–sea ice hindcasts performed over the period 1960–2015 (hereafter OCCITENS), and in a one-member 330-year climatological simulation (hereafter OCCICLIM). In this context, OCCITENS simulates both the intrinsic and forced variability, while OCCICLIM simulates the "pure" intrinsic variability. We explore several features of the KE, finding analogies between the OCCICLIM and OCCITENS datasets with autonomous and non-autonomous dynamical systems respectively. This approach aims to apply concepts from the dynamical systems theory on complex and realistic ocean simulations. In this framework, the results suggest that both oceanic and atmospheric drivers control the KE LFV, and that the effect of the low-frequency atmospheric forcing reduces the phase space region explored by the system through synchronization mechanisms. The system's intrinsic variability can be paced, and therefore clustered over the system's pullback attractor under the effect of the time dependent forcing.

## 1 Introduction

The Kuroshio Extension (KE) is the eastward flowing meandering jet east of Japan formed by the confluence of the Kuroshio and Oyashio western boundary currents (WBCs; e.g., Qiu 2001). The KE region is known for the highest Eddy Kinetic Energy (EKE) level in the North Pacific Ocean (Wyrтки et al. 1976), whose changes lead to large sea–surface temperature anomalies that are able to enhance the variability of the midlatitude coupled ocean–atmosphere system (e.g., Latif and Barnett 1994, 1996; Zhang and Luo 2017).

It is widely mentioned in the literature that the KE variability is bimodal on interannual to decadal time scales (e.g. Chao 1984; Qiu 2000, 2002), shifting between two main states: (i) the elongated state, in which the jet is fairly stable, zonally elongated with two anticyclonic meanders east of Japan and (ii) the contracted state, in which the jet is zonally contracted, much more convoluted and during which the two anticyclonic meanders are fed by an inverse cascade

✉ Giusy Fedele  
giusy.fedele@cmcc.it

<sup>1</sup> Department of Environmental Science, Informatics and Statistics, Cà Foscari University, Venice, Italy

<sup>2</sup> Ocean Modeling and Data Assimilation Division (ODA), Centro Euro-Mediterraneo sui Cambiamenti Climatici, Bologna, Italy

<sup>3</sup> Institut des Géosciences de l'Environnement, Centre National de la Recherche Scientifique, Saint-Martin-d'Hères, France

<sup>4</sup> Parthenope University of Naples, Naples, Italy

<sup>5</sup> Climate Simulation and Prediction Division (CSP), Centro Euro-Mediterraneo sui Cambiamenti Climatici (CMCC), Bologna, Italy

<sup>6</sup> Department of Physical, Chemical and Natural Systems (SFQN), University Pablo de Olavide (UPO), Seville, Spain

<sup>7</sup> Consiglio Nazionale delle Ricerche, Istituto di Scienze dell'Atmosfera e del Clima, Bologna, Italy

energy process (Qiu and Chen 2005, 2010). It has also been observed that the KE's low frequency variability (LFV) can affect the location and strength of the North Pacific storm track (Zhang and Luo 2017) and some studies also report impacts of the KE LFV on the Asian and North American Climate (e.g., Latif and Barnett 1994, 1996; Qiu 2000). It is therefore climatologically relevant to understand the nature of this bimodality and to investigate the predictability properties of the phenomenon.

The nature of the KE LFV is still under debate with complementary views regarding the respective roles of the ocean's intrinsic variability and of the atmospheric variability in driving the quasi-decadal variability of the jet (e.g., Pierini and Dijkstra 2009).

In the first view the KE LFV is driven by internal dynamics involving the nonlinear interactions between recirculations, potential vorticity advection and eddies (e.g. Jiang et al. 1995; Dijkstra and Ghil 2005; Pierini 2006). Using simple idealized double-gyre models forced by constant winds, other studies (Pierini 2006; Pierini et al. 2009; Gentile et al 2018) found the two KE LFV regimes to be in agreement with altimetry data (Qiu 2003; Qiu and Chen 2005, 2010), supporting the intrinsic origin of the phenomenon.

According to an alternative view, the KE LFV shows a significant synchronization with large-scale atmospheric variability modes, such as the Pacific Decadal Oscillation (PDO) and the North Pacific Gyre Oscillation (see Miller et al. 1998; Deser et al. 1999; Mantua and Hare 2002; Qiu 2003; Qiu and Chen 2005; Ceballos et al. 2009). Using an eddy-resolving ocean general circulation model (OGCM), Taguchi et al. (2007) showed that the KE LFV is linked with the propagation of Rossby waves from the East-Central Northern Pacific driven by the large-scale atmospheric variability. It has also been shown that changes in the KE jet speed are associated with frontal-scale variability that is likely generated by internal ocean dynamics, suggesting that linear Rossby waves may explain the jet's temporal variability, while nonlinear ocean dynamics may organize its spatial structure (Taguchi et al. 2007; Nonaka et al. 2012). It was also suggested that shifts from the elongated state to the convoluted one are linked to the eastward propagation of potential vorticity anomalies from the western boundary current region (Cessi et al. 1987). Dewar (2003) and Hogg et al. (2005) also identified a mode of intrinsic variability of the wind-driven double gyre system, in which slow adjustments of the potential vorticity field are associated with meridional shifts in the jet position at decadal timescales.

These two views may nevertheless be reconciled, as suggested by Pierini (2014a), who interpreted the KE LFV as a case of intrinsic variability paced by an external forcing. Using an eddy-resolving OGCM under the perfect-model assumption, Nonaka et al. (2012) have investigated the potential predictability of interannual variability in the

KE jet speed related to the westward propagation of wind-driven oceanic Rossby waves. They observed a modest interannual predictability of the KE jet speed fluctuations (only 46% of its total variance) associated with the Rossby waves propagation. They suggested two possible reasons for this limited predictability: the influence of wind variations in the western North Pacific that can reduce predictability at longer lead times, and the presence of internal variability that is uncorrelated with atmospheric forcing, and can yield randomness in the KE jet variability.

In this work we investigate the role of the intrinsic ocean variability and of the atmospheric fluctuations in the KE LFV adopting the perspective of dynamical systems theory. We analyze a large ensemble of eddy-permitting global ocean/sea-ice hindcasts driven by the same atmospheric forcing from different initial conditions, and a single-member long climatological one-member simulation. By construction, the climatological simulation isolates the quasi-autonomous (i.e., forced by a repeated seasonal cycle) or "pure" KE intrinsic variability, while the ensemble simulation represents the non-autonomous (atmospherically-modulated) KE intrinsic variability. These two forms of variability are non additive in such a highly nonlinear framework, but a preliminary analysis of this kind does shed light on their respective contributions to the total signal.

We will first use a classical approach to disentangle the intrinsic and forced oceanic LFV from the ensemble simulation. The ensemble mean fluctuations will provide an estimate of the forced, deterministic variability induced by the atmospheric forcing shared by all members; the ensemble spread around the ensemble mean, measured by the time-varying ensemble standard deviations, will provide an estimate of the intrinsic and chaotic variability generated by the turbulent ocean at this eddy-permitting resolution.

In a second approach, we will analyze the KE LFV from time-varying ensemble probability density functions (PDFs), which provide a probabilistic description of the time-varying impact of the atmospheric variability on the jet's intrinsic variability in the non-autonomous regime. The climatological simulation will be compared with the ensemble simulation using a similar paradigm, but in a context where the atmospheric forcing is quasi-autonomous and no longer modulates the LFV of the KE attractor. This approach will allow us to describe the KE LFV in a reduced phase space, interpret its evolution in a realistic context in the light of (quasi) autonomous and non-autonomous dynamical systems theory and provide insights into the system's predictability.

Section 2 describes our datasets, the indices and post-processing tools we used to characterize the KE behavior, and provides an assessment of the ensemble

simulation realism. In Sect. 3 the results obtained by the two approaches are presented. Conclusions are finally drawn in Sect. 4.

## 2 Datasets, post-processing and model assessment

### 2.1 Datasets

All the simulations used in this study were performed during the OCCIPUT (Oceanic Chaos—Impacts, Structure, Predictability; see Penduff et al. 2014) project with the same NEMO3.5 ocean/sea-ice model setup. The global configuration uses a  $1/4^\circ$  horizontal resolution (grid spacing of 27 km at the equator, decreasing poleward) and a 75-level vertical discretization (Bessières et al. 2017). We make use of two OCCIPUT datasets: a 50-member ensemble hindcast (hereafter OCCITENS) performed over the period 1960–2015, and a companion one-member 330-year long climatological simulation (hereafter OCCICLIM).

All members of the OCCITENS ensemble are forced by the same 6-hourly DRAKKAR forcing set DFS5.2 (Dussin et al. 2016), which is based on the ERA-40 and ERA-Interim reanalyses and includes the full range of atmospheric timescales over this period. On the other hand, OCCICLIM is forced by a repeated annual cycle derived from DFS5.2, and devoid of any interannual or synoptic variability. The use of this seasonal forcing (which retains the contribution of the main quadratic air-sea flux terms as explained in Penduff et al. 2011) in OCCICLIM instead of a constant forcing ensures that key seasonal processes are at work and maintain the model mean state (water mass structure, overturning circulation, etc.) with a seasonal variability that is very close to that obtained under a fully-varying forcing (see Gregorio et al. 2015). Regardless of the timescales retained in the variability of prescribed atmospheric fields, the air-sea fluxes applied to each member of OCCITENS ensemble and in the OCCICLIM run

partly depend on the SST field that is simulated at each timestep within each model experiment, consistently with the classical bulk forcing method (see Sect. 2 in Brodeau et al. 2010). OCCICLIM thus provides insight into the pure intrinsic variability that spontaneously emerges from the ocean. The characteristics of both simulations are summarized in Table 1. More details are given in Leroux et al. (2018), where OCCITENS and OCCICLIM were labeled as ENSx50-occi025 and CLIM-occi025, respectively.

Starting from a one-member 21-yr spinup simulation, the 50 members of the OCCITENS ensemble hindcast are initialized in 1960 by activating a small stochastic perturbation in the equation of state within each member (Brankart et al. 2015; Bessières et al. 2017). This stochastic perturbation is only applied for the first year (1960) to seed the ensemble dispersion, and remains switched off for the rest of the ensemble hindcast (from 1961 to 2015). Once the stochastic perturbation is stopped at the end of 1960, the 50 members are thus integrated from slightly perturbed initial conditions and forced by the same atmospheric conditions until 2015. Our diagnostics are performed from 5-daily simulated sea-surface height (SSH) fields over the 1980–2015 period, since the DFS5.2 forcing does not include any interannual variability in the buoyancy fluxes before 1980. This choice yields a total effective spinup time of 41 years within each member.

The OCCITENS sea-level variability is assessed against the AVISO dataset (Archiving, Validation, and Interpretation of Satellite Oceanographic data; see <http://www.aviso.altimetry.fr>, and the AVISO User Handbook) which provides daily sea level anomaly (SLA) data on a  $0.25$ -degree grid on the 1993–2017 period. Adding the Mean Absolute Dynamic Topography (MADT) provided by AVISO to these SLA fields gives the total SSH fields. The next section presents how the observed and simulated SSH fields were post-processed and used to derive additional variables and indices.

**Table 1** Model setups and simulations

	Main characteristics of the simulations used in this study	
	OCCITENS	OCCICLIM
Domain	Global	Global
NEMO version	3.5	3.5
Resolution	$1/4^\circ$ and 75 vertical levels	$1/4^\circ$ and 75 vertical levels
Type	Ensemble hindcast	Climatological
No. of members (N)	50	1
Atmospheric forcing	DFS5.2 (all time scales)	Repeated annual cycle from DFS4
Time period	1960–2015	330 yr
References:	Bessières et al. (2017) and Leroux et al. (2018)	

## 2.2 Post-processing

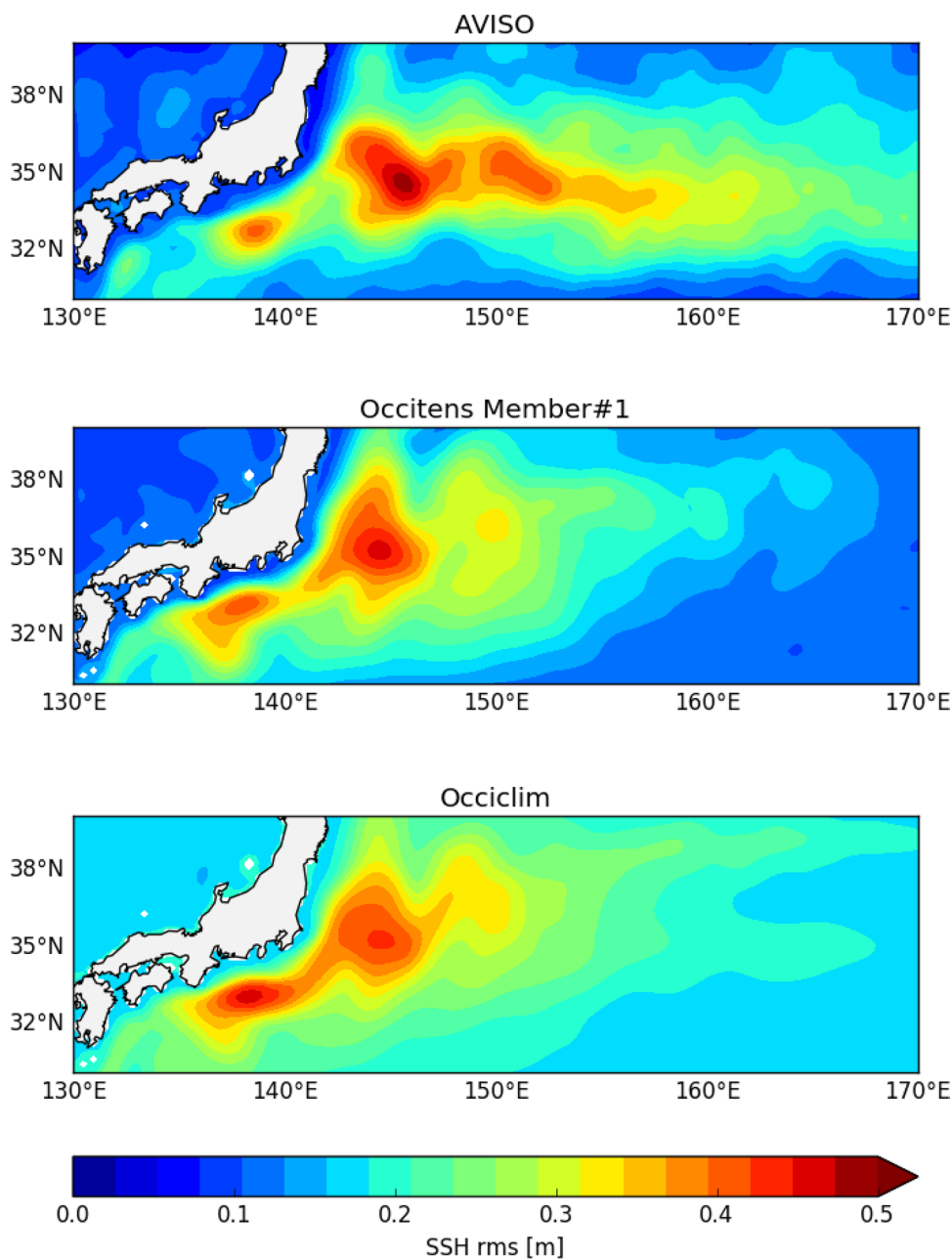
### 2.2.1 Indices

The KE LFV has been characterized by various scalar indices in the past (e.g. Qiu and Chen 2005, 2010; Pierini 2006, 2015). We use modeled and observed SSH fields, geostrophic surface velocity (GSV) fields derived from SSH gradients and the Coriolis parameter to calculate four scalar indices characterizing the KE every 5 days: the KE velocity (KE<sub>vel</sub>), the KE eddy kinetic energy, the KE Length (LKE), and the KE mean latitudinal position ( $\bar{\phi}$ ).

The longitudinal range 141–153°E used to evaluate the various KE indices in the “Upstream KE region” is a classical choice first introduced by Qiu and Chen (2005) and later used by many authors. We adopted the same range since despite small biases in our model solutions, it captures most of the SSH variance in the KE region in our simulation and in the observations (Fig. 1). The KE<sub>vel</sub> index is calculated at every latitude between 32 and 38°N as the maximum amplitude of GSV integrated zonally in the Upstream KE region (141–153°E), where eddy-eddy interactions and the jet variability are strongest (Fig. 1; Qiu and Chen 2005):

$$KE_{vel} = \max_{32,38^{\circ}N} \langle |GSV| \rangle_{141,153^{\circ}E}. \quad (1)$$

**Fig. 1** Standard deviations of 5-days SSH (m) for AVISO (top), for one ensemble member of OCCITENS (center) and for OCCICLIM (bottom)



EKE fields are deduced from GSV fields as

$$EKE = \frac{1}{2} \mathbf{u}' \cdot \mathbf{u}', \tag{2}$$

where  $\cdot$  is the scalar product and  $\mathbf{u}'$  is the vector for the eddy component of the GSV field, defined as departures from the mean annual cycle. The EKE index is then obtained by averaging EKE over the region [141–153°E; 32–38°N].

The  $\bar{\phi}$  and LKE indices are derived from the pathway of the Kuroshio axis in the upstream KE region (141–153°E). The Kuroshio axis is defined as the SSH isoline where the meridional SSH gradient is maximum on average over this region; these isolines correspond to the SSH values 0.7 m in the simulations and 0.9 m in the observations. The  $\bar{\phi}$  and LKE indices are, therefore, the latitude and length of the Kuroshio axis averaged zonally over the upstream KE region. Various observational studies have shown that the KE indices are not independent: during the elongated state the jet is located north and LKE and EKE are small, while in the convoluted state the jet shifts southward and the LKE and EKE increase (Qiu and Chen 2005, 2010; Pierini 2006, 2014a, b). The behavior of the model regarding these observed features is commented later in the paper.

### 2.2.2 The OCCICLIM pseudo ensemble

To perform a consistent comparison of the evolution of these four scalar indices in OCCITENS and in OCCICLIM, we split the last 300-year (ignoring the first 30 years of spinup) single OCCICLIM time series into fifty 36-year intervals, hence yielding a pseudo-ensemble having the same structure and size as the OCCITENS ensemble. Each interval starts on the first day (January 1st) of a random year of the original OCCICLIM time series, and therefore represents a 36-year realization of the pure intrinsic variability.

The pure (quasi-autonomous) intrinsic variability of the KE will be characterized by the evolution of the four scalar indices derived from the OCCICLIM pseudo-ensemble, and compared to its atmospherically-modulated counterpart derived from OCCITENS. This comparison will help characterizing the role of the full atmospheric variability in exciting, damping, or pacing the pure intrinsic variability, using concepts of dynamical systems theory as done previously with simpler numerical simulations. The OCCITENS ensemble and the OCCICLIM pseudo-ensemble are further processed and analyzed using the same approaches and tools, which are described below.

### 2.2.3 Low-pass filtering and nonlinear detrending

These four scalar indices were computed from 5-daily fields for the ensemble simulation, the climatological simulation, and the observations. In order to focus on the KE

interannual-to-decadal variability, these time series were low-passed filtered using a LOWESS (Locally Weighted Scatterplot Smoothing) operator with a 1-yr cutoff period.

The statistical analysis (e.g. variance, spectra, correlation estimations) of time series may be biased due to two possible causes. First, geophysical time series often include timescales that are longer than their actual duration (e.g. multi-decadal variability, trends, etc.); second, time series derived from primitive equation model simulations often contain long-term, possibly nonlinear, spurious drifts due to mismatches between model initial states and forcing fields, or to missing processes. We deal with both issues by applying to all time series a LOWESS nonlinear detrending operator, which is similar to (but more computationally-efficient than) the LOESS operator used by Leroux et al (2018) for the same purpose. This operator is applied to the four scalar indices derived from the OCCITENS ensemble and the OCCICLIM pseudo ensemble (as shown in Fig. 2). The application of the same low-pass filtering and nonlinear detrending operators to all time series guarantees that all signals analyzed in the following are trend-free, and devoid of periods longer than 36 years and shorter than 1 year.

### 2.2.4 First approach: a simple estimate of the forced and intrinsic variabilities

This section summarizes the first method (see Leroux et al 2018 for more information) we used to analyze the OCCITENS dataset in terms of forced and intrinsic variabilities. Any pre-processed OCCIPUT-derived time series  $f_i(t)$ ,  $i = 1, N$  (either model outputs or any of the indices introduced above) in member  $i$  may be written as:

$$f_i(t) = \langle f \rangle(t) + f'_i(t), \tag{3}$$

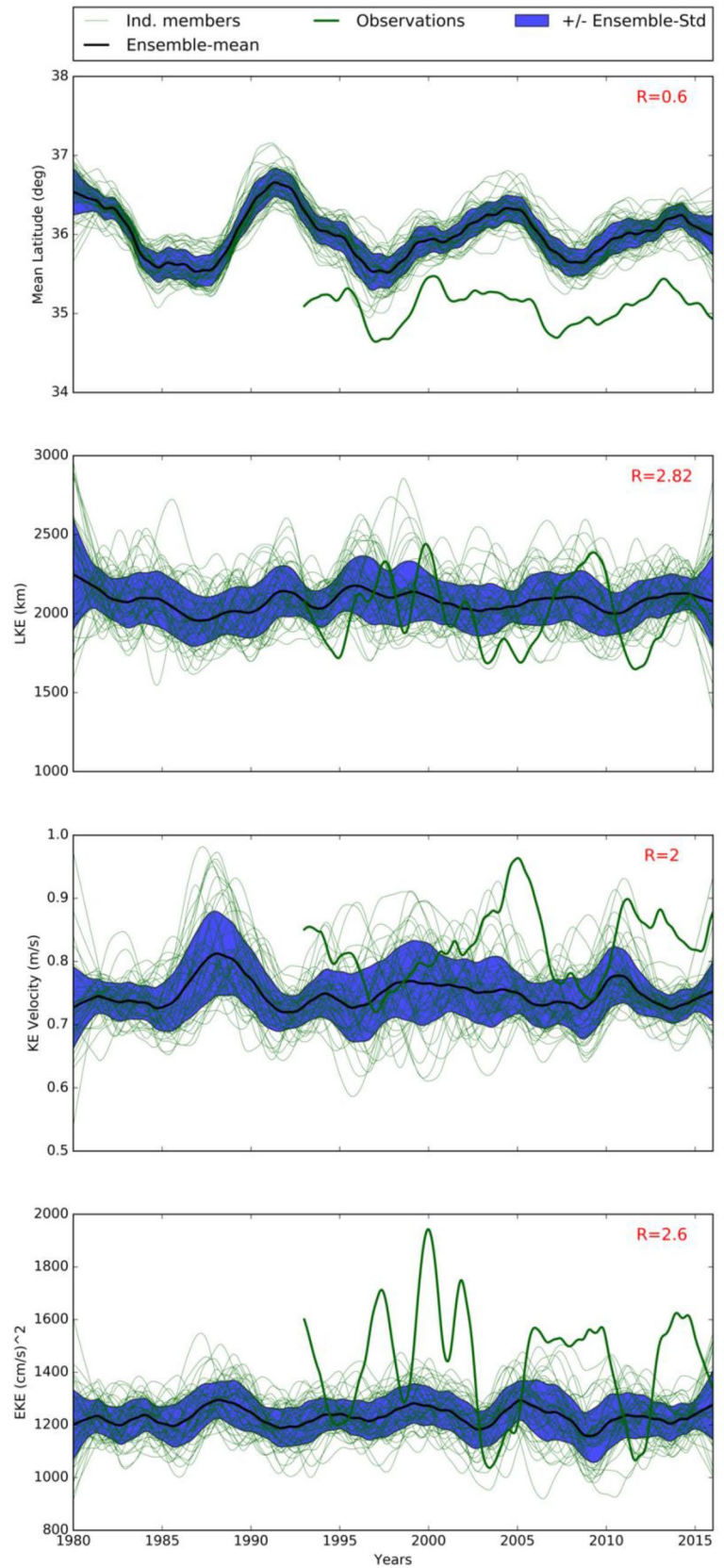
where  $N$  is the number of members, angled brackets denote the ensemble mean (an estimator of the atmospherically-forced signal) and prime superscript represent the intrinsic signal in member  $i$ . The total, forced and intrinsic variabilities ( $A_{total}$ ,  $A_{forced}$ ,  $A_{intrinsic}$ , respectively) may thus be estimated as:

$$\begin{cases} A_{total} = \langle \sigma_f \rangle \\ A_{forced} = \sigma_{\langle f \rangle} \\ A_{intrinsic} = \sqrt{\bar{\epsilon}^2} \end{cases}, \tag{4}$$

where  $\sigma_f$  is the temporal standard deviation of time series  $f$ ,  $\bar{\epsilon}^2$  is the (time-varying) ensemble variance of the  $N$   $f_i$  samples, and the overbar is the temporal averaging operator. It can be shown that  $A_{total}^2 = A_{forced}^2 + A_{intrinsic}^2$ . The amplitude ratio  $R = \frac{A_{intrinsic}}{A_{forced}}$  will provide a simple estimate of the relative contributions of intrinsic variability and



**Fig.2** Time series of the low pass filtered, detrended KE indices (mean latitudinal position, LKE, KE velocity, and EKE from top to bottom) from ENSx50-occi025. The 50 individual trajectories are shown as thin green lines; the ensemble mean evolutions are shown as thick black lines; ensemble standard deviations are shaded. The amplitude ratio  $R$  is indicated at the top right. The observed evolution of the 4 indices is shown as green lines



atmospherically-forced variability to the total variability of signal  $f$ . Note that the same statistics may be applied to the OCCICLIM pseudo-ensemble, where by construction at interannual-to-decadal timescales the variability is purely intrinsic and the forced variability  $A_{\text{forced}}$  should be close to zero at interannual time scales.

Figure 2 shows for the four scalar indices derived from OCCITENS, the forced signals (black lines), the ensemble standard deviation  $\sigma$  (half-width of the blue bands) and the amplitude ratio  $R$ . The forced variability exceeds the intrinsic variability ( $A_{\text{intrinsic}} = 0.6A_{\text{forced}}$ ) only for  $\bar{\phi}$ : the interannual-to-decadal variability of the mean latitudinal position of the KE is mostly atmospherically-driven. In contrast, the interannual-to-decadal variability of LKE, KEvel and EKE is predominantly intrinsic ( $R = 2.82, 2$  and  $2.6$  respectively), indicating that the atmospheric variability is only a secondary driver of these KE features.

### 2.2.5 Limitations of this first approach

This first approach makes the assumptions that the oceanic variability in an ensemble like OCCITENS may be split into forced and intrinsic variabilities, and that their respective evolutions may be described from the first and second moments of a variable's ensemble PDF. These two assumptions are made very often and have yielded interesting results for the study of the coupled ocean–atmosphere and of the oceanic variability (see e.g. Drijfhout and Hazeleger 2007; Sérazin et al. 2017; Leroux et al. 2018). One may pragmatically consider that these assumptions are reasonable when the time-varying ensemble PDF of the variable under consideration remains close to Gaussian (or at least symmetric) over time; in this quasi-Gaussian case, the first two statistical moments of an ensemble PDF indeed provide an almost complete description of the system's evolution, and the splitting between forced and intrinsic variabilities is made implicitly.

In the framework of the dynamical system theory the trajectories of ensemble members are analyzed in the phase space, where they wrap around the system's pullback attractor (PBA). The attractor is stationary in the autonomous case (constant forcing), while it is constantly distorted (possibly in complex ways) by the variable external forcing in non-autonomous cases (see e.g. Pierini et al. 2018; Pierini 2019). The simple method presented above would actually be consistent with this more rigorous paradigm in special cases, e.g. when the system's attractor constantly remains quasi-Gaussian for the variable under consideration and when the fluctuating atmospheric forcing modulates the attractor's center of gravity ( $C_g$ ) in phase space (variable ensemble mean i.e. forced variability) but not the attractor's shape (intrinsic variability subspace). The  $C_g$  is here defined as the location of the median of the distribution in the phase space.

Generally, and consistently with the central limit theorem, time-varying ensemble PDFs of temporally and/or spatially integrated quantities (like SSH long-term trends, or interannual AMOC time series) are much closer to Gaussian than those of very local and instantaneous variables (see e.g. Fig. 2 in Penduff et al. 2018). Llovel et al. (2018) used a Lilliefors test to show that the ensemble PDFs of local sea-level trend estimates derived from the 50 OCCIPUT members are indeed close to Gaussian over most of the global ocean area, hence allowing a simple and complete description of the ensemble statistics via their mean and standard deviation. We used the same Lilliefors test to assess the Gaussianity of the time-varying ensemble PDFs of the four KE indices throughout the 36-year OCCITENS dataset: the results show that during 79–91% of this period (depending on the index), the 5-daily ensemble PDFs are indeed Gaussian at 95% confidence. In other words, the evolution of these indices may be characterized most of the time from time-varying ensemble mean and ensemble STD; this simple approach will be used as a preliminary step below.

However, when the time-varying ensemble PDF of a variable often happens to be non-Gaussian, this simple description of the variability may be incomplete and its splitting into forced and intrinsic components may be questionable. In such cases, concepts and techniques derived from the theory of non-autonomous dynamical systems can provide complementary and more mathematically-grounded descriptions of the system behavior. We will propose in Sect. 3 an attempt in this direction, with additional diagnostics inspired from such concepts.

### 2.3 Assessment of the KE LfV in OCCITENS

The KE LfV in OCCITENS is now assessed by comparing the 50-member evolution of the four scalar indices with the evolution of their observed counterpart (see Fig. 2). As explained in Leroux et al (2018), the observed variability may be also seen as a single realization of the real ocean evolution, and is very likely to include a random component that is out of phase with most of its simulated realizations.

The latitudinal position  $\bar{\phi}$  of the KE appears to be shifted to the north by about  $1^\circ$  in all OCCITENS members; this overshoot of western boundary currents is typical of eddy-permitting simulations, and had been already noted in  $1/4^\circ$  global NEMO simulations (e.g. Penduff et al. 2010; Fedele et al. 2021). However this bias does not forbid the study of the variability itself. As noted above, the interannual-to-decadal fluctuations of the jet latitude are predominantly controlled by the atmospheric variability: the ensemble mean  $\langle \bar{\phi} \rangle$  clearly exhibits forced fluctuations, which do resemble the observed signal. This impact of the forcing on the low-frequency KE latitude is likely to be mediated by the propagation of long Rossby waves across the Pacific

(e.g. Qiu and Chen 2005, 2010; Sasaki et al. 2013), as discussed below.

The typical length (LKE  $\sim$  2200 km) of the observed KE is well simulated in the model, but its typical EKE and velocity are smaller than observed, as expected in eddy-permitting simulations (Fig. 2b–d). The interannual-to-decadal variability of these three indices was shown to be mostly intrinsic, as confirmed by their large random dispersion around their ensemble mean. The intrinsic origin of LKE and EKE fluctuations may be due to the large imprint of the random eddy field on these indices. The KEvel variability is expected to be sensitive to the eddy field as well (through e.g. rectification; Nonaka et al. 2012), but is slightly more sensitive to the forcing variability ( $R=2$ ), presumably since it is related more directly to the jet's latitudinal shifts as shown in Sect. 3.

The realism of the OCCITENS ensemble simulation is now assessed against the observed interannual-to-decadal variability of the four KE indices over the common available

period (1993–2015). Results are summarized in Fig. 3 as Taylor diagrams (Taylor 2001), which exhibit the temporal correlation coefficients, STD ratios and RMS errors between each modeled time series and their observed counterparts. The correlation coefficients between the KE mean latitude  $\bar{\phi}$  in each member and the observations span a very large range (0.1–0.8), and reach the largest values in members where the intrinsic variability phase happens to better match its observational counterpart. The  $\bar{\phi}$  STD ratios exhibit a large inter-member diversity as well (0.7–1.6), but their ensemble average is close to the observational estimate. This large span between members illustrates the strong sensitivity of model-observation comparisons on a particular model realization, and demonstrates the poor robustness of such a comparison when only one eddying model integration is available. As the ensemble averaging operator suppresses the intrinsic "noise" from simulated time series, the ensemble mean (atmospherically-forced) variability exhibits a smaller

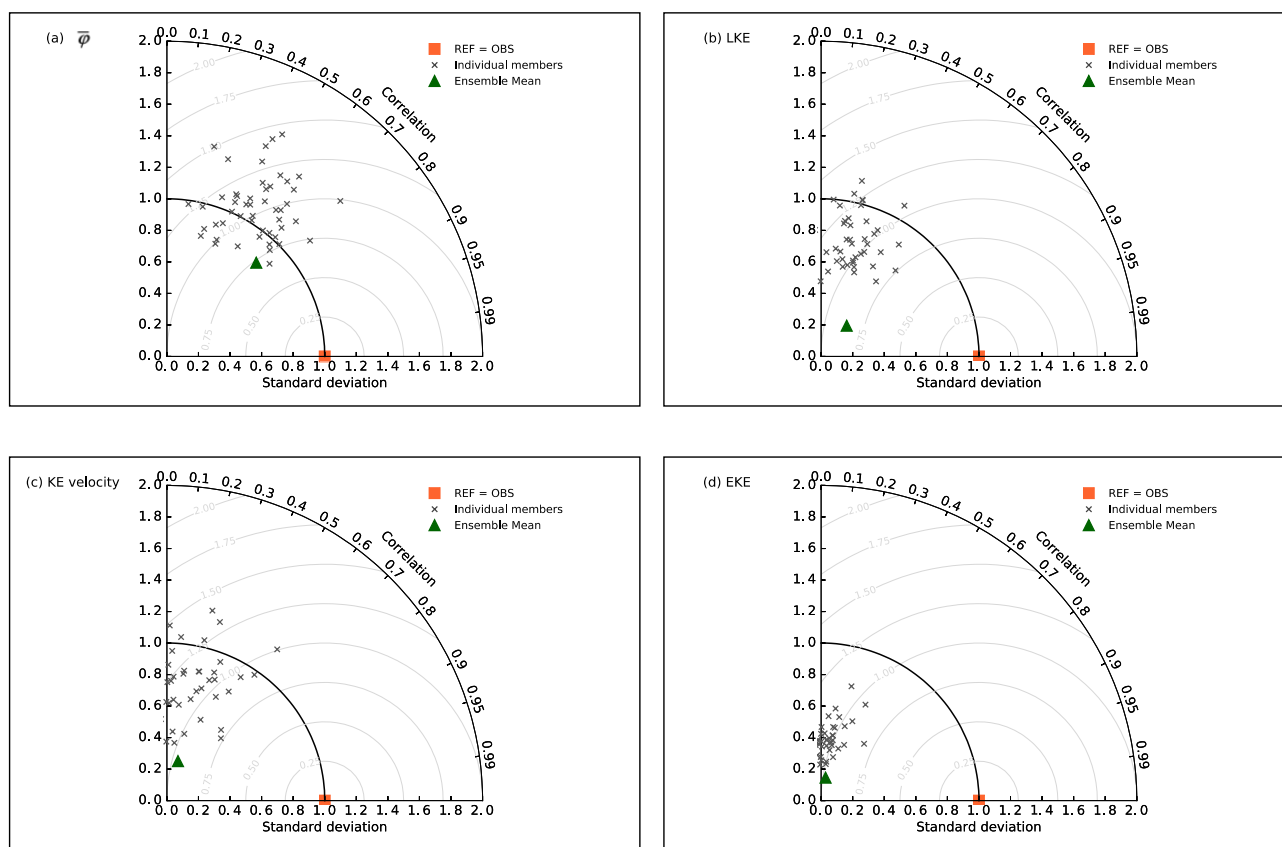


**Fig. 3** Assessment of the low-pass filtered (LPF) 1993–2015 evolution of the KE indices in the OCCITENS ensemble by means of Taylor diagrams (Taylor 2001). The references are the LPF 1993–2015 evolution of the 4 indices in the AVISO observational timeseries. Results are shown for the KE mean latitudinal position (a), length (b), velocity (c), and EKE (d). Black crosses correspond to the 50 individual members, and green triangles to their ensemble mean;

for each of these symbols, the angle with the horizontal axis shows the correlation with the observed time series, the radial distance to the origin shows the ratio of their temporal standard deviations with respect to the observation, and the radial distance to the reference point (orange square) corresponds to the RMS error between observed and simulated time series



STD ratio (and a larger correlation with observations) than most individual realization.

The fluctuations of the KE velocity and length reach about 70% of their observed amplitude on average over the ensemble, again with a large inter-member scatter due to the larger contribution of intrinsic processes to these indices' variabilities. The cloud of points clearly shrinks toward the origin for the EKE interannual-to-decadal variability, as the model only represents about 40% of its observed magnitude. The limited STD ratios and simulation-observation correlations found within each member and for their ensemble mean may be partly explained by model imperfections due to its limited resolution or its forcing; nevertheless, it is equally likely that these features can be explained by the strong imprint of intrinsic variability on both simulated and (presumably) observed quantities.

To summarize, these Taylor diagrams provide a rather complete view of the interannual-to-decadal KE variability in the OCCITENS ensemble, and highlight the importance of intrinsic, random fluctuations of the system. The model correctly simulates the deterministic part of the interannual-to-decadal variability of the KE latitude, with a tendency to underestimate the eddy variability.

### 3 The KE LfV: intrinsic versus forced variability mechanisms

We have shown in the previous section that both the intrinsic and forced components contribute to the total low-frequency variability of the KE; in particular, the external forcing influences the broad-scale latitudinal variability of the KE latitude more than the frontal-scale variability (velocity, EKE, length), which is more influenced by intrinsic fluctuations. Further investigation is still required to identify the mechanisms involved in this phenomenon. We first examine in Fig. 4 the SLA time series computed for every member in the PDO center of action (32–34° N, 175–180° W), the longitude-time Hovmöller diagram of the ensemble mean (forced) SLA in both the upstream and downstream regions, and the forced LKE anomaly with respect to its mean value. The latitudinal band has been chosen in order to highlight the teleconnection mechanism between the KE and the PDO center of action (e.g. Mantua and Hare 2002; Newman et al. 2016; Fedele et al. 2021). In this respect, several studies show that the SLA variability over the KE recirculation gyre (south of the KE jet, 32°–34°N; e.g. Qiu 2003; Qiu and Chen 2005, 2010; Ceballos et al. 2009; Andres et al. 2009; Wang et al. 2016) is strongly connected with the signal driven by the PDO in the east-central Pacific: when the PDO gets stronger (weaker), negative (positive) Rossby waves propagate westward and the recirculation gyre gets

weaker (stronger). This choice is therefore adequate to highlight this mechanism.

The SLA signal forced by the atmosphere between 175 and 180°W is almost in phase within all members. This signal then travels westwards toward the KE extension at a speed of about 4 cm/s; this suggests a teleconnection mechanism via baroclinic Rossby wave trains between wind-driven SLA perturbations in the East-Central Pacific and the Upstream KE region. Further connections appear in this western part of the basin: the remotely-forced negative SLA anomalies correspond with positive ensemble-mean LKE anomalies, which then seem to excite shifts from the elongated state to the convoluted state. These atmosphere-driven modulations are in agreement with observations (i.e. Qiu and Chen 2005, 2010).

The highest correlation between the forced SLA evolution between 175 and 180°W (Fig. 4) and the ensemble mean latitudinal position index (Fig. 2) reaches ~0.61 and is found at a 3 yrs lag ( $p$  value  $\leq 0.05$ ). This lag indeed corresponds to the time needed for baroclinic Rossby waves to propagate from the East-Central Northern Pacific to the west.

Complementary features are shown in Fig. 5, which presents latitude-time Hovmöller diagrams of the SLA averaged in the upstream KE region in the observations and in the model (ensemble mean and one member of OCCITENS).

Marked differences can be seen between the SLA evolution in a random OCCITENS member (hereafter member #1, right panel) and in the real ocean (left panel), as expected from the strong SLA imprint of intrinsic variability in the KE region. This strong imprint of intrinsic variability is directly illustrated by the difference between total and forced SLA signals in OCCITENS (compare panels c and b): intrinsic variability explains why total SLA fluctuations are much stronger than their forced counterparts. Despite the strong imprint of intrinsic variability in member #1 and presumably in observations, the 3 panels of Fig. 5 suggest concomitant shifts in the latitude of the KE maximum velocity at interannual-to-decadal time scales, such as in 1993–1996 or after 2009. These correspondences illustrate the partial constraint exerted by the atmosphere on the simulated and real Kuroshio, in agreement with the previous analyses. An equatorward propagation of SLA anomalies is also found in the model along the timeseries, in agreement with Yang and Liang (2016), who found that shifting from the elongated to the convoluted state, the jet moves southward, while the two quasi-stationary anticyclonic circulations in the KE are attenuated through energy conversion processes and an equatorward eddies propagation.

The same analysis shown in Fig. 6 for the GSV fields provides a qualitative confirmation that the interannual-to-decadal latitudinal shifts of the jet are partly atmospherically driven. More specifically, comparing the yearly averaged AVISO GSV (Fig. 6a) with the OCCITENS ensemble mean

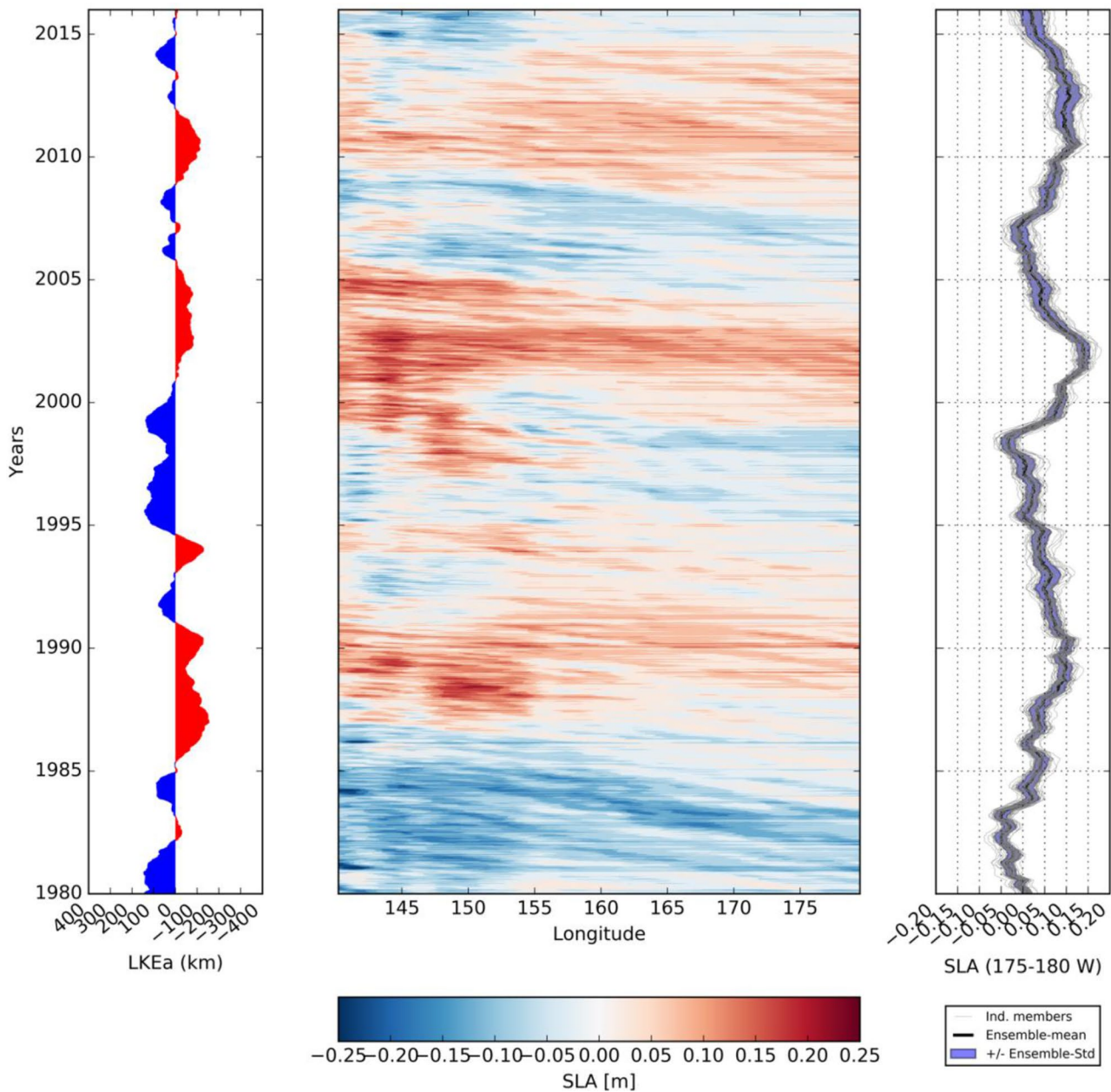


**Fig. 4** Left: ensemble mean LKE anomaly (LKEa) (negative values in red, positive values in blue). Center: Hovmöller diagram of the ensemble mean SLA averaged over 32–34° N. Right: Low pass

filtered SLA averaged between 32–34° N—175–180° W for the 50 ensemble members (thin gray lines) and for the ensemble mean (thick black line); the ensemble standard deviation is shaded

(Fig. 6b) highlights some discrepancies as well as some significant agreement. First of all, the ensemble mean exhibits weaker KE velocities than observed, but this is mainly due to the averaging procedure; in fact, the velocities within a single ensemble member (Fig. 6d) are comparable to those of the original AVISO data (Fig. 6c).

Coming back to Fig. 6a, b, one can identify four time intervals with specific characteristics. In A the ensemble mean reveals a gradual southward shift of the KE jet followed by a northward shift while the altimeter data show

a more variable signal which, nonetheless, does include episodes of southward migration. In B a fairly stable mean upstream KE jet located at  $\sim 35.5^\circ$  is present in both datasets. In C a weaker jet, shifted to the south and fairly variable, is again present in both datasets. Finally, in D the modeled mean jet shows a northward migration, again consistent with AVISO data.

Overall, the significant agreement evidenced by these two datasets may be seen as an interesting statistical model validation in the considered area (the statistical character of

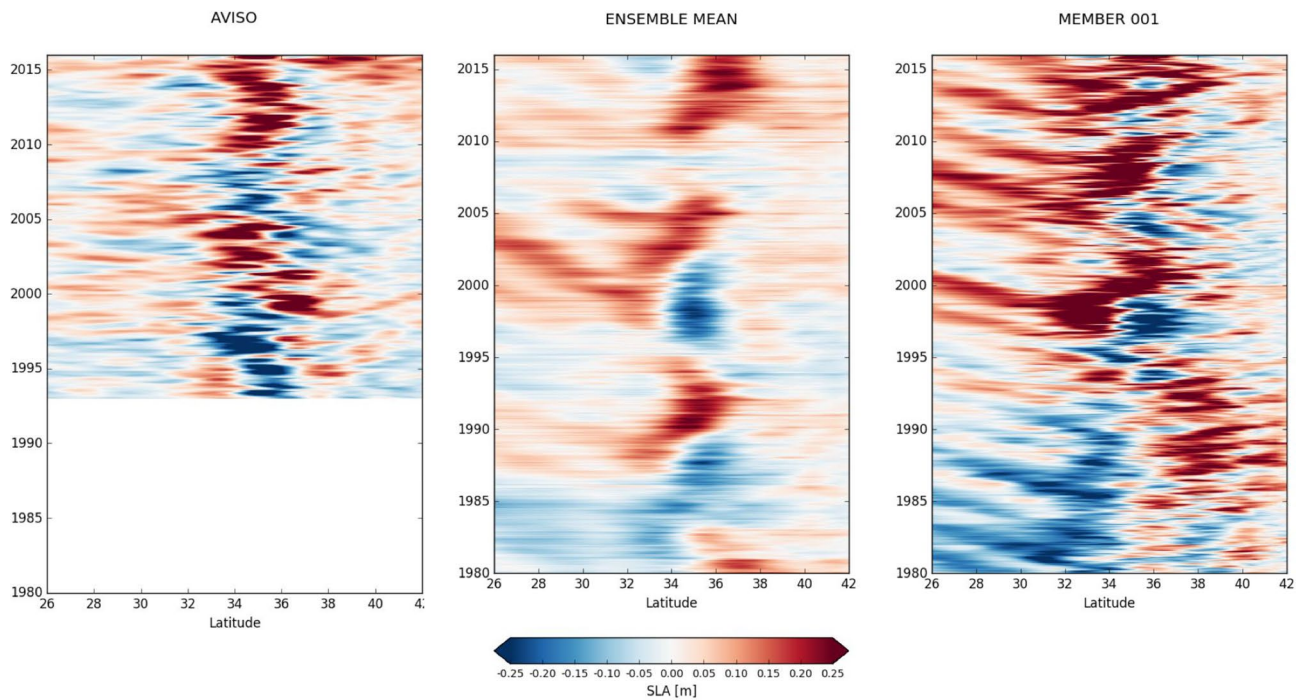


**Fig. 5** SLA Hovmöller diagrams in the latitude-time domain (averaged in the upstream KE region) for AVISO (left), the ensemble mean (center) and one ensemble member (right)

the validation refers here to the ensemble mean performed over the OCCITENS dataset). In the same statistical sense, the pacing effect of the atmospheric forcing (remotely acting through Rossby wave dynamics) prevails over the intrinsic mechanisms driving the jet fluctuations.

It is worth stressing that these conclusions hold only in a statistical sense. Indeed, no significant coherency emerges if a single ensemble member (Fig. 6d) is compared with the original AVISO altimeter data (Fig. 6c). This is compatible with the typical chaotic nonautonomous dynamical systems' behavior according to which the trajectories in phase space may be mutually uncorrelated, but they all lie on the system's PBA (e.g., see Pierini 2014b and Fig. 3a therein for an example of this behavior). This interesting aspect, evidenced for the first time in the framework of a realistic oceanic ensemble simulation, will be further investigated in a future study.

### 3.1 The pure intrinsic KE variability in OCCICLIM: analogies with autonomous dynamical systems

In order to assess the roles of the atmospheric forcing and of intrinsic ocean processes in modulating the KE features, we now take advantage of the climatological run OCCICLIM, which isolates the KE pure intrinsic variability under seasonal forcing. Comparing the OCCITENS ensemble with the OCCICLIM pseudo-ensemble should allow us to better

assess the impact of the fully-variable forcing on the jet's intrinsic variability. Since aperiodically forced systems are nonergodic (Drotos et al. 2016), the OCCILIM pseudo-ensemble cannot be considered as a rigorous equivalent to an actual ensemble simulation such as OCCITENS, where the members differ by their initialization; their comparison will nonetheless be shown to be very useful in the following discussion.

In this section we start from Fig. 6, which highlights the link in OCCITENS between the LFV variability of the KE velocity and latitude; this figure will help us investigate the relationships between both variables, as well as their sensitivity to the atmospheric variability. We compute in OCCICLIM (then in OCCITENS) the time-varying Joint Probability Distributions (JPD) of the KE indices in the two-dimensional  $\Phi$ - $\Psi$  phase-space, where  $\Phi$  is given by the jet's latitude, and  $\Psi$  by KEvel. This approach will allow us to characterize probabilistically the links between the jet's large-scale latitudinal variability (which is mainly driven by the atmosphere in OCCITENS) and the jet's frontal-scale variability related to  $\Psi$  (which is mainly driven by internal mechanisms). We first investigate the JPD evolution in the OCCICLIM simulation, and discuss possible analogies with the evolution of autonomous dynamical systems (i.e. the KE under quasi-stationary forcing). We acknowledge that the OCCICLIM seasonal forcing is not stationary, so that the associated



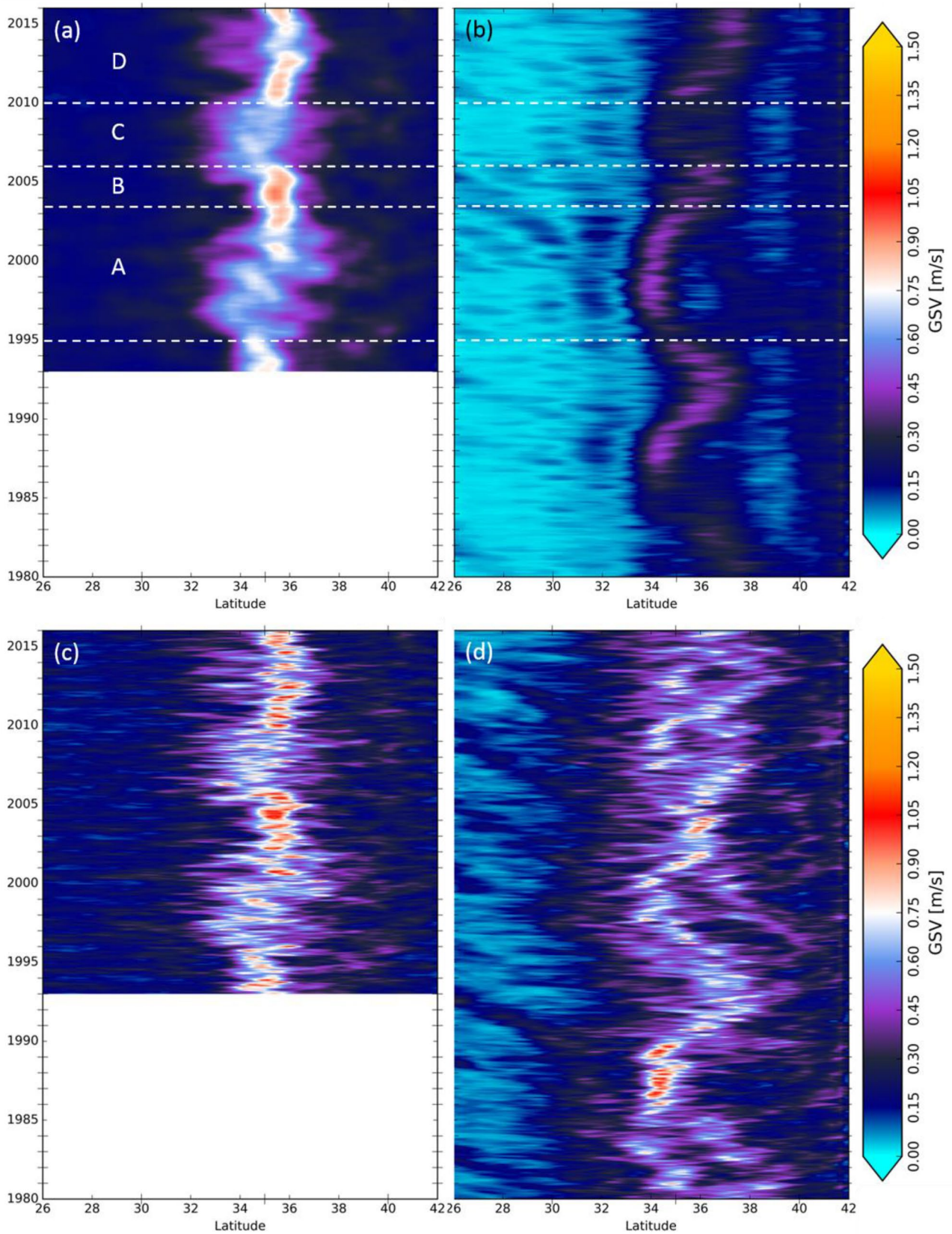


**Fig. 6** Hovmöller diagram of the GSV in the latitude-time domain averaged in the upstream KE region. **a** Yearly averaged AVISO data. **b** OCCITENS ensemble mean. **c** AVISO data. **d** First OCCITENS ensemble member

KE dynamics may not be rigorously seen as a genuinely autonomous system. However, we focus on timescales that are longer than 1 year, over which the OCCICLIM forcing is constant; in addition, the ocean's low-frequency intrinsic variability was shown by Sushama et al. (2007) to be weakly sensitive to the atmospheric seasonal cycle. For these two reasons, it may be relevant and interesting to compare the interannual-to-decadal intrinsic KE variability in OCCICLIM and in an autonomous dynamical system.

We compute time-varying JPDs over 36 successive 1-year time series extracted from the 50-member OCCICLIM pseudo-ensemble. JPDs give a simple (two-dimensional) and probabilistic description of the high-dimensional KE system state over successive years. The bin sampling ( $20 \times 20$  bins) has been chosen to split the latitude domain ( $34\text{--}39^\circ\text{N}$ ) into clusters comparable to the horizontal model resolution. Figure 7 shows three of these yearly JPDs, which all exhibit the bimodal character of the KE pure intrinsic variability: in the absence of any interannually-varying forcing, the system tends to occupy the same two preferred regions of the  $\Phi$ - $\Psi$  phase space, which differ by the jet's latitude ( $37\text{--}38^\circ\text{N}$  and  $35.5\text{--}36.5^\circ\text{N}$ ) but share the same range of  $\Psi$  values. These results support the idea that intrinsic ocean dynamics are

responsible for the bimodal distribution of the latitude PDF under seasonal forcing.

JPDs are very likely impacted by under-sampling due to the limited size of the OCCICLIM pseudo-ensemble each year; successive JPDs may therefore differ because of this undersampling. However, the 36 JPDs built from the OCCICLIM pseudo-ensemble are very similar, indicating that although the KE evolution has a random evolution within each individual pseudo-member (i.e. over individual 36-year chunks of the seasonally-forced simulation), the probabilistic description of the system's state does not evolve much in  $\Phi$ - $\Psi$  phase space. The initial spread in the OCCITENS ensemble is by construction smaller than that in the OCCICLIM pseudo-ensemble, as for ensembles initialized with microscopic vs macroscopic initial condition uncertainties (ICUs, see Stainforth et al. 2007). However, the OCCITENS spreads in 1980–2015 on which we focus have saturated at larger values, which are very comparable to those found by Gehlen et al (2020) in an OCCITENS-like ensemble initialized with macroscopic ICUs. This strongly suggests that differences found between OCCITENS and OCCICLIM are not due to different initializations, but to dynamical processes as expected in such non-linear dynamical systems. To assess

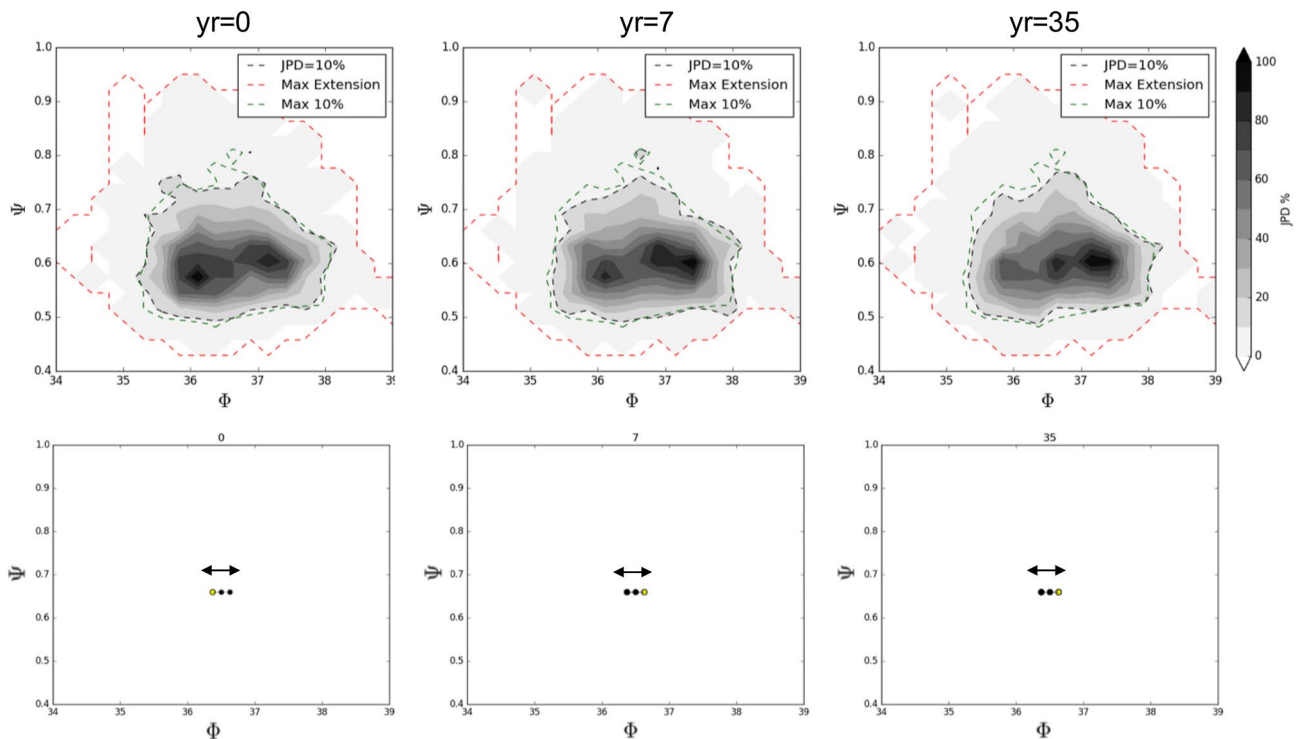


**Fig. 7** Upper panels: yearly Joint Probability Distributions (JPD, gray shading) of the KE mean latitudinal position ( $\Phi$ ) and velocity ( $\Psi$ ) in the OCCICLIM pseudo-ensemble at years 0, 7, and 35. The yearly 10% deciles are shown as black dashed lines. The red and green dashed lines are the same in the 3 upper panels, and show the first

decile of the  $\Phi$ - $\Psi$  JPD computed over the full 36-year OCCICLIM pseudo-ensemble (0% and 10% isolines are shown in red and green, respectively). Lower panels: position of the center of gravity of the JPDs at each selected year (yellow dots) and over the full 36-year OCCICLIM pseudo-ensemble (black dots)



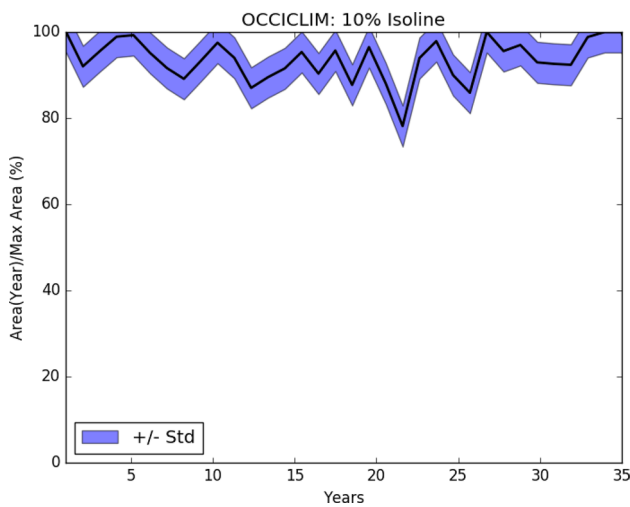


**Fig. 8** Ratio between the area surrounded by yearly 10% isolines and the maximum area explored by the 10% isoline during the 36-years time series in the OCCICLIM pseudo-ensemble. The width of the blue shading is twice the temporal standard deviation of this ratio

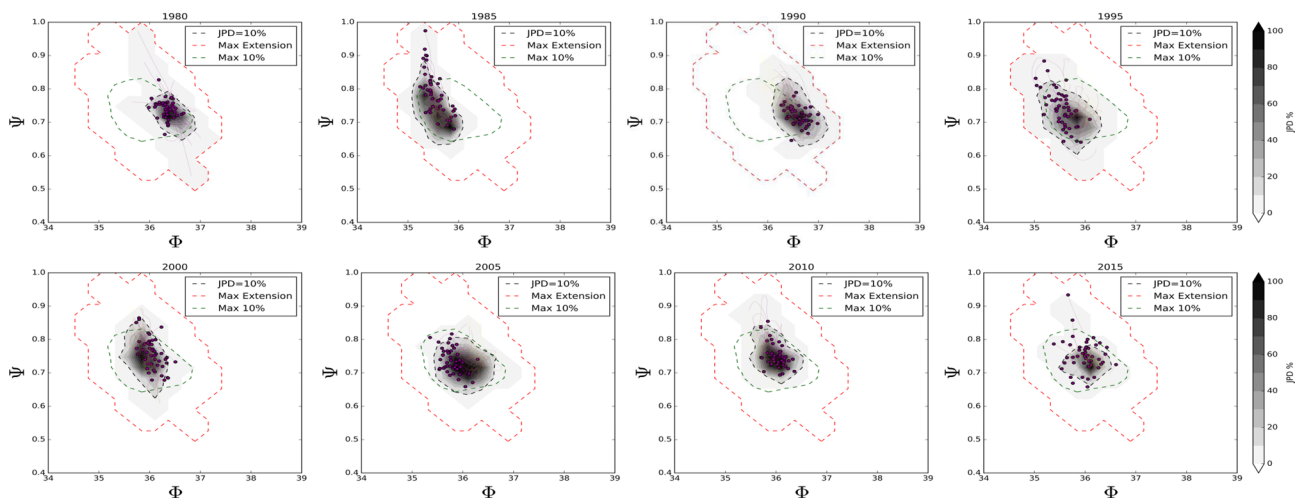
this evolution, we computed the ratio between the area surrounded by yearly 10% isolines and the maximum area explored by the 10% isoline during the 36-years time series in the OCCICLIM pseudo-ensemble (Fig. 8). Changes in the JPDs' Cg (bottom panels in Fig. 7) and area (Fig. 8) over time are much smaller in OCCICLIM than those in OCCITENS (see below), and small enough to state that the interannual fluctuations of the KE under seasonal forcing are rather consistent with the time-independence of the system's attractor. It is however very likely that increasing

the number of members or pseudo-members would yield a more precise and stable set of JPDs.

### 3.2 The atmospherically-modulated intrinsic KE variability in OCCITENS: analogies with nonautonomous dynamical systems

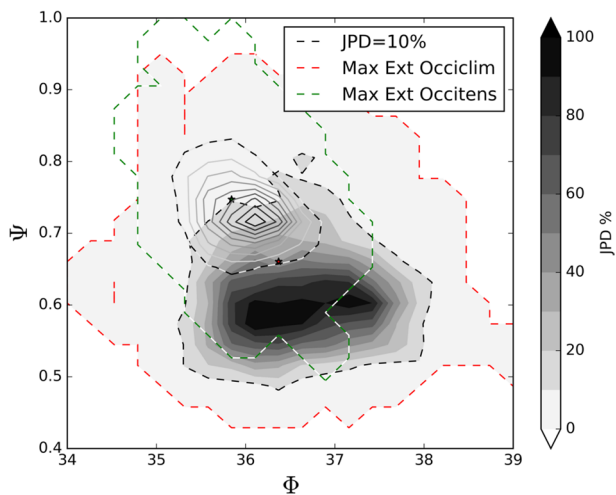
The way the atmospheric variability influences the KE intrinsic variability is now investigated from the indices' time series derived from the 50-member OCCITENS ensemble: yearly JPDs are derived from these data in the  $\Phi$ - $\Psi$  space, as done for OCCICLIM. Their evolution is now influenced by both the fully-variable atmospheric forcing and the oceanic chaotic variability; it may thus be interesting to interpret their evolution in the light of non-autonomous (i.e. atmospherically-modulated) dynamical systems, now taking advantage of the full, potentially complex (e.g. non-Gaussian), markedly evolving structure of the joint ensemble statistics that is shown in Fig. 9.

Figure 9 shows that when a fluctuating external forcings is applied on the ocean model, both the intrinsic and forced contributions modulate the shape the JPDs in the  $\Phi$ - $\Psi$  phase space. The projection of the PBA on this phase space occupies a region that is much smaller in the OCCITENS than in the OCCICLIM case (Fig. 10). This is likely due to synchronization mechanisms through which the variable forcing can notably reduce the ensemble spread, and which are obviously absent in the quasi-autonomous case. For example, the ensemble spread of the low-order excitable ocean model of Pierini (2011) subject to an aperiodic decadal-time-scale forcing yields a substantial reduction in particular temporal



**Fig. 9** Yearly JPDs (gray shading) of the KE mean latitudinal position ( $\Phi$ ) and velocity ( $\Psi$ ) in the OCCITENS ensemble every 5 year over the period 1980–2015. The yearly 10% deciles are shown as black dashed lines. The red and green dashed lines are the same in all panels and show the first decile of the  $\Phi$ - $\Psi$  JPD computed over the

full 36-year OCCITENS ensemble (0% and 10% isolines are shown in red and green, respectively). The purple lines show the evolution of the KE in this  $\Phi$ - $\Psi$  phase space for each of the 50 members during each selected year; the state of the KE at the end of each selected year is shown for each member as purple dots



**Fig. 10** JPDs of the KE mean latitudinal position ( $\Phi$ ) and velocity ( $\Psi$ ) computed over the full 36-year OCCICLIM pseudo-ensemble (gray shadings) and OCCITENS ensemble (gray contours). The 10% deciles are shown as black dashed lines for both datasets. The maximum extensions of both JPDs (0% deciles) are shown in red and green for OCCICLIM and OCCITENS, respectively. The red/green star indicates the OCCICLIM/OCCITENS center of gravity

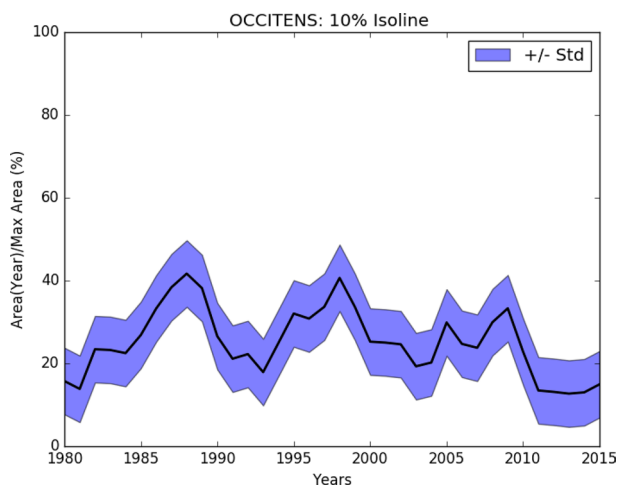


**Fig. 11** Same as Fig. 8 for the OCCITENS ensemble

ranges (see Pierini 2019, and Fig. 4b therein). This occurs when the time dependent forcing induces a strong synchronization of the intrinsic system’s relaxation oscillations present in the various ensemble members with the forcing itself. A similar but less dramatic behavior appears to be acting in the OCCITENS dataset.

Figure 11 shows that the bimodality in OCCITENS is not as clear as in OCCICLIM, where the two modes are distinct meridionally but similar in terms of velocity. This smaller bimodality and smaller latitudinal fluctuations of the KE in OCCITENS come along with statistically larger velocities; this finding is consistent with observational studies (e.g. Qiu

and Chen 2005) which have shown that a stronger (weaker) KE velocity tends to be associated with a more stable (unstable) KE path.

In contrast with OCCICLIM, the JPD evolution in OCCITENS is affected by the action of the external forcings. Figure 9 shows that the KE evolutions in the different members follow nearby trajectories in this phase space. The closer the trajectories between the members, the larger the atmospheric constraint on the KE evolution and the smaller the contribution of the intrinsic chaotic variability. The fluctuating nature of this atmospheric constraint is illustrated in Fig. 11, which shows the ratio between the area explored by the 10% instantaneous isoline each year and the maximum area explored by the 10% JPD throughout the whole OCCITENS analysis period (1980–2015). This ratio remains around 20–25% throughout the analysis period but exceeds the 40% threshold occasionally, suggesting that in such a nonautonomous system individual trajectories can strongly diverge in certain cases.

In this context, the JPDs provide a measure of the density of the trajectories inside the attractor, but they say nothing about the phase. This information has been derived by computing the locations occupied by the Cg of the distributions in the phase space (Fig. 12). Sixteen positions of the Cg are identified in the 36-yr OCCITENS time series. Here it is shown that between the 1980–1991 and 2001–2010 periods, the system evolves in a clockwise direction in the  $\Phi$ - $\Psi$  plane, and anticlockwise between 1991–2000 and 2011–2015 time-frames. The opposite phases of the orbits indicate that there is not a prior direction in the phase space, in agreement with the study by Gentile et al. (2018). They showed a similar behavior in AVISO analyzing the 1993–2016 time series (i.e. anticlockwise direction between 1994–1998 and clockwise direction between 1998–2006). The evolution of the simulated KE over the analysis period is thus consistent with actual observations.

### 4 Conclusions

This study is devoted to the analysis of the KE LfV in a large ensemble of eddy-permitting global ocean-sea ice hindcasts. In the first part of the work, we followed a usual method based on simple statistical moments (means and variances) to disentangle the forced and intrinsic variabilities. Results show a strong dependence of the mean latitudinal position on the atmospheric variability, in contrast with the other indices (LKE, EKE, KEvel) which are more sensitive to intrinsic oceanic variability. In other words, the atmosphere partly controls the jet’s latitude, but the ocean’s intrinsic variability strongly modulates the jet’s frontal variability. These features have been investigated in more detail in the second part of the work, where a new approach has

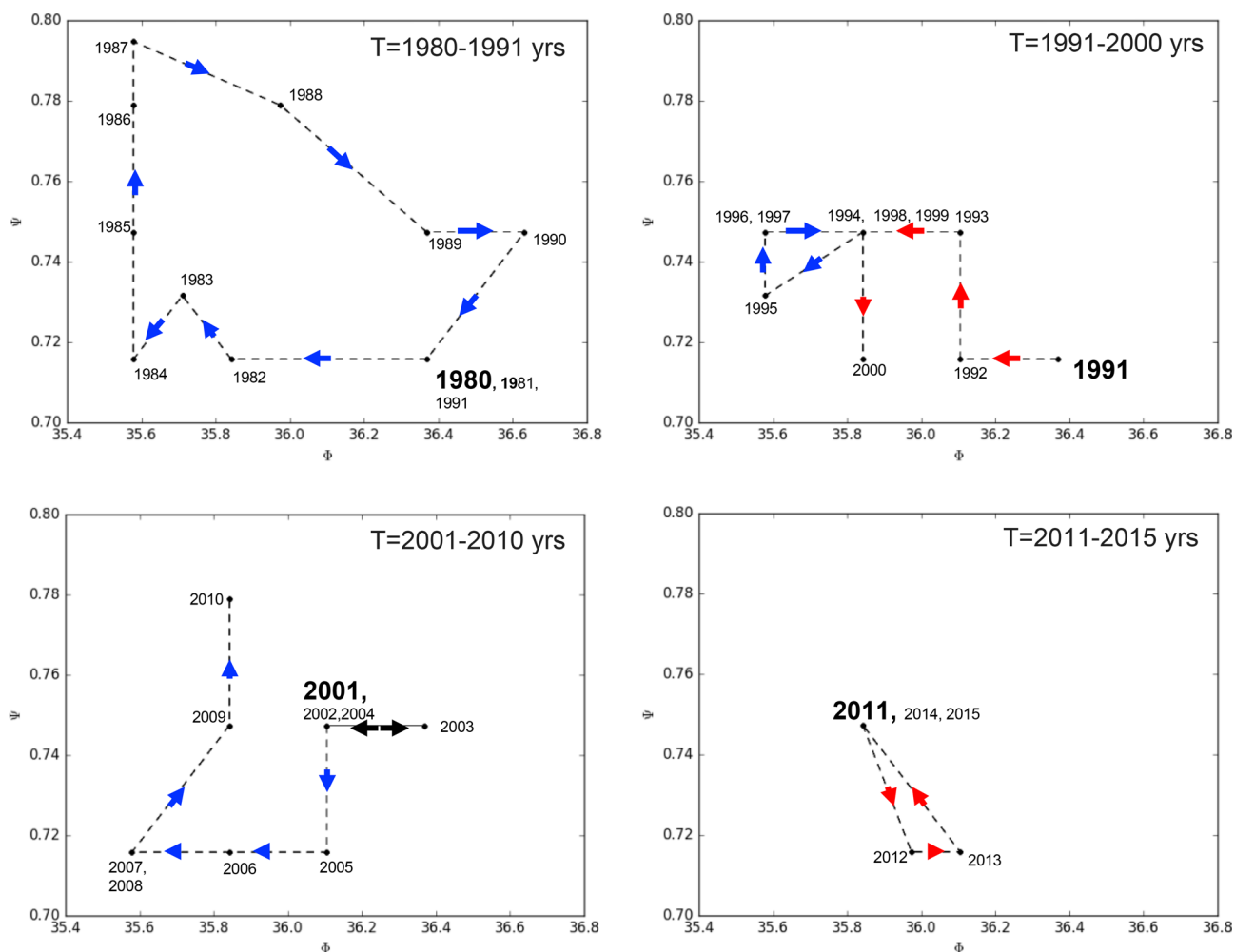


**Fig. 12** Evolution in the OCCITENS ensemble of the center of gravity of yearly JPDs (black dots) in the mean latitudinal position ( $\Phi$ )—velocity ( $\Psi$ ) phase space. The 36-year evolution is split into 4 peri-

ods: **a** 1980–1991, **b** 1991–2000, **c** 2001–2010 and **d** 2011–2015. The first year of the loop is indicated in bold. Clockwise and anticlockwise loops are shown in blue and red, respectively

been proposed. We took advantage of the analogies between the OCCICLIM and OCCITENS datasets with autonomous and non-autonomous dynamical systems, respectively. In this study we confirm previous results but also make some steps forward in the understanding of this phenomenon. Our results support the hypothesis that the KE LFV is shaped by intrinsic oceanic mechanisms, and that its phase is paced by the external forcing in agreement with Pierini (2014a). The bimodality of the jet is well captured by OCCICLIM: this supports the intrinsic origin of the low-frequency fluctuations of the jet position. Of course, no phase agreement with the real data is expected in OCCICLIM because the atmospheric forcing lacks the LFV needed to pace the intrinsic KE variability. On the other hand, significant phase agreement is found between the OCCITENS ensemble mean, resulting from the full atmospheric forcing, and altimeter observations.

Many differences were then found between the latitude-velocity JPDs in OCCICLIM and OCCITENS, which are therefore due to the fluctuation of the external forcings. More precisely, we showed that in the non-autonomous case (full atmospheric variability), the KE explores a more restricted region of the latitude-velocity phase-space: the atmospheric variability acts reducing the size of the KE attractor in the analyzed domain. This suggests a possible synchronization mechanism between the forced and intrinsic variabilities that constrain the trajectories in restricted regions of phase space.

Moreover, while in the climatological run the KE oscillates between two main modes through a transition phase, the KE jet explores the phase space following different directions under fully-variable forcing, in agreement with updated altimeter observations (Gentile et al. 2018).

Future investigations would certainly benefit from ensemble simulations at finer resolution, which would likely yield more consistent eddy dynamics and more realistic

representations of the KE dynamics and variability. Our suggested approach would also benefit from the availability of larger ensembles. The computational resources required for increasing both resolution and ensemble size in global primitive equation models would however be huge for today's standards. In the meantime, our results nevertheless demonstrate the potential of jointly analyzing ocean simulation ensembles such as OCCITENS and available observations for the study of non-linear ocean dynamics modulated by complex atmospheric fluctuations. Identifying the implications of our results for the coupled ocean-atmospheric system is another important issue, which is left for the future.

**Acknowledgements** The results of this research have been achieved using the PRACE Research Infrastructure resource CURIE based in France at TGCC. This work is a contribution to the OCCIPUT and PIRATE projects. OCCIPUT has been funded by ANR through contract ANR-13-BS06-0007-01. PIRATE is funded by CNES through the Ocean Surface Topography Science Team (OST-ST). The model dataset used for this study is available on request (Thierry.Penduff@cns.fr). This work was part of the G.F. PhD in "Science and Management of Climate Change" of the Cà Foscari University of Venice. We acknowledge the CMCC Foundation for having provided computational resources for performing model diagnostics. The authors wish to thank two anonymous reviewers, whose constructive comments helped improve the paper.

## References

- Andres M, Park JH, Wimbush M, Zhu XH, Nakamura H, Kim K, Chang KI (2009) Manifestation of the Pacific decadal oscillation in the Kuroshio. *Geophys Res Lett* 36:L16602
- Bessièrès L, Leroux S, Brankart J-M, Molines J-M, Moine M-P, Bouttier P-A, Penduff T, Terray L, Barnier B, Sérazin G (2017) Development of a probabilistic ocean modelling system based on NEMO 3.5: application at eddy resolution. *Geosci Model Dev* 10:1091–1106. <https://doi.org/10.5194/gmd-10-1091-2017>
- Brankart J-M, Candille G, Garnier F, Calone C, Melet A, Bouttier P-A, Brasseur P, Verron J (2015) A generic approach to explicit simulation of uncertainty in the NEMO ocean model. *Geosci Model Dev* 8:1285–1297. <https://doi.org/10.5194/gmd-8-1285-2015>
- Brodeau L, Barnier B, Penduff T, Treguier A-M, Gulev S (2010) An ERA40-based atmospheric forcing for global ocean circulation models. *Ocean Model* 31:88–104. <https://doi.org/10.1016/j.ocemod.2009.10.005>
- Ceballos LI, Di Lorenzo E, Hoyos CD, Schneider N, Taguchi B (2009) North Pacific Gyre Oscillation synchronizes climate fluctuations in the eastern and western boundary systems. *J Clim* 22:5163–5174
- Cessi P, Ierley GR, Young WR (1987) A model of the inertial recirculation driven by potential vorticity anomalies. *J Phys Oceanogr* 17:1640–1652
- Chao S-Y (1984) Bimodality of the Kuroshio. *J Phys Oceanogr* 14:92–103. [https://doi.org/10.1175/1520-0485\(1984\)014,0092:BOTK.2.CO;2](https://doi.org/10.1175/1520-0485(1984)014,0092:BOTK.2.CO;2)
- Deser C, Alexander MA, Timlin MS (1999) Evidence for a wind-driven intensification of the Kuroshio current extension from the 1970s to the 1980s. *J Clim* 12:1697–1706
- Dewar WK (2003) Nonlinear midlatitude ocean adjustment. *J Phys Oceanogr* 33:1057–1082. [https://doi.org/10.1175/1520-0485\(2003\)033<1057:NMOA>2.0.CO;2](https://doi.org/10.1175/1520-0485(2003)033<1057:NMOA>2.0.CO;2)
- Dijkstra AH, Ghil M (2005) Low-frequency variability of the large-scale ocean circulation: a dynamical systems approach. *Rev Geophys* 43:RG002
- Drijfhout SS, Hazeleger W (2007) Detecting Atlantic MOC changes in an ensemble of climate change simulations. *J Clim* 20:1571–1582. <https://doi.org/10.1175/JCLI4104.1>
- Dussin R, Barnier B, Brodeau L, Molines J-M (2016) The making of Drakkar forcing set DFS5. DRAKKAR/MyOcean Report, 01–04-16. LGGE, Grenoble
- Fedele G, Bellucci A, Masina S, Pierini S (2021) Decadal variability of the Kuroshio extension: the response of the jet to increased atmospheric resolution in a coupled ocean–atmosphere model. *Clim Dyn* 56:1227–1249. <https://doi.org/10.1007/s00382-020-05528-4>
- Gehlen M, Berthet S, Séférian R, Ethé C, Penduff T (2020) Quantification of chaotic intrinsic variability of sea-air CO<sub>2</sub> fluxes at interannual timescales. *Geophys Res Lett*. <https://doi.org/10.1029/2020GL088304>
- Gentile V, Pierini S, de Ruggiero P, Pietranera L (2018) Ocean modelling and altimeter data reveal the possible occurrence of intrinsic low-frequency variability of the Kuroshio extension. *Ocean Model* 131:24–39. <https://doi.org/10.1016/j.ocemod.2018.08.006>
- Gregorio S, Penduff T, Serazin G, Molines J-M, Barnier B, Hirschi J (2015) Intrinsic variability of the Atlantic meridional overturning circulation at interannual-to-multidecadal timescales. *J Phys Oceanogr* 45:1929–1946. <https://doi.org/10.1175/JPO-D-14-0163.1>
- Hogg AM, Killworth PD, Blundell JR, Dewar WK (2005) Mechanisms of decadal variability of the wind-driven ocean circulation. *J Phys Oceanogr* 35:512–531
- Jiang S, Jin FF, Ghil M (1995) Multiple equilibria, periodic, and aperiodic solutions in a wind-driven, double-gyre, shallow-water model. *J Phys Oceanogr* 25:764–786
- Latif M, Barnett TP (1994) Causes of decadal climate variability over the North Pacific and North America. *Science* 266:634–637
- Latif M, Barnett TP (1996) Decadal climate variability over the North Pacific and North America: dynamics and predictability. *J Clim* 9:2407–2423
- Leroux S, Penduff T, Bessièrès L, Molines J, Brankart J, Serazin G, Barnier B, Terray L (2018) Intrinsic and atmospherically forced variability of the AMOC: insights from a large-ensemble ocean hindcast. *J Clim* 31:11831203
- Lllovel W, Penduff T, Meyssignac B, Molines J-M, Terray L, Bessièrès L, Barnier B (2018) Contributions of atmospheric forcing and chaotic ocean variability to regional sea level trends over 1993–2015. *Geophys Res Lett* 45:13405–13413. <https://doi.org/10.1029/2018GL080838>
- Mantua NJ, Hare SR (2002) The Pacific decadal oscillation. *S R J Oceanogr* 58:35. <https://doi.org/10.1023/A:1015820616384>
- Miller AJ, Cayan DR, White WB (1998) A westward-intensified decadal change in the North Pacific thermocline and gyre-scale circulation. *J Clim* 11:3112–3127
- Newman M, Alexander MA, Ault TR, Cobb KM, Deser C, Di Lorenzo E, Mantua NJ, Miller AJ, Minobe S, Nakamura H, Schneider N, Vimont DJ, Phillips AS, Scott JD, Smith CA (2016) The Pacific decadal oscillation. *Rev J Clim* 29:4399–4427. <https://doi.org/10.1175/JCLI-D-15-0508.1>
- Nonaka M, Sasaki H, Taguchi B, Nakamura H (2012) Potential predictability of interannual variability in the Kuroshio extension jet speed in an eddy-resolving OGCM. *J Clim* 25:3645–3652
- Penduff T, Juza M, Brodeau L, Smith GC, Barnier B, Molines J-M, Treguier A-M, Madec G (2010) Impact of global ocean model resolution on sea-level variability with emphasis on interannual



- time scales. *Ocean Sci* 6:269–284. <https://doi.org/10.5194/os-6-269-2010>
- Penduff T, Juza M, Barnier B, Zika J, Dewar WK, Treguier A-M, Molines J-M, Audiffren N (2011) Sea level expression of intrinsic and forced ocean variabilities at interannual time scales. *J Clim* 24:5652–5670
- Penduff T, Barnier B, Terray L, Bessières L, Sérazin G, Gregorio S, Brankart J, Moine M, Molines J, Brasseur P (2014) Ensembles of eddy ocean simulations for climate, CLIVAR Exchanges, Special Issue on High Resolution Ocean Climate Modelling, 19
- Penduff T, Sérazin G, Leroux S, Close S, Molines J-M, Barnier B, Bessières L, Terray L, Maze G (2018) Chaotic variability of ocean heat content: climate-relevant features and observational implications. *Oceanography*. <https://doi.org/10.5670/oceanog.2018.210>
- Pierini S (2006) A Kuroshio extension system model study: decadal chaotic self-sustained oscillations. *J Phys Oceanogr* 36:1605–1625
- Pierini S (2011) Low-frequency variability, coherence resonance and phase selection in a low-order model of the wind-driven ocean circulation. *J Phys Oceanogr* 41:1585–1604. <https://doi.org/10.1175/JPO-D-10-05018.1>
- Pierini S (2014a) Kuroshio extension bimodality and the North Pacific Oscillation: a case of intrinsic variability paced by external forcing. *J Clim* 27:448–454
- Pierini S (2014b) Ensemble simulations and pullback attractors of a periodically forced double-gyre system. *J Phys Oceanogr* 44(12):3245–3254. <https://doi.org/10.1175/jpo-d-14-0117.1>
- Pierini S (2015) A comparative analysis of Kuroshio extension indices from a modeling perspective. *J Clim* 28(14):5873–5881. <https://doi.org/10.1175/JCLI-D-15-0023.1>
- Pierini S (2019) Statistical significance of small ensembles of simulations and detection of the internal climate variability: an excitable ocean system case study. *J Stat Phys*. <https://doi.org/10.1007/s10955-019-02409-x>
- Pierini S, Dijkstra AH (2009) Low-frequency variability of the Kuroshio extension. *Nonlin Processes Geophys* 16:665–675
- Pierini S, Dijkstra AH, Riccio A (2009) A nonlinear theory of the Kuroshio extension bimodality. *J Phys Oceanogr* 39:2212–2229
- Pierini S, Chekroun MD, Ghil M (2018) The onset of chaos in non-autonomous dissipative dynamical systems: a low-order ocean-model case study. *Nonlin Processes Geophys* 25:671–692. <https://doi.org/10.5194/npg-25-671-2018>
- Qiu B (2000) Interannual variability of the Kuroshio extension system and its impact on the wintertime SST field. *J Phys Oceanogr* 30:1486–1502
- Qiu B (2001) Kuroshio and Oyashio Currents. *Encyclopedia of Ocean Sciences*, Academic Press, 1413–1425
- Qiu B (2002) The Kuroshio Extension system: Its large-scale variability and role in the midlatitude ocean–atmosphere interaction. *J Oceanogr* 58:57–75
- Qiu B (2003) Kuroshio Extension variability and forcing of the Pacific decadal oscillations: responses and potential feedback. *J Phys Oceanogr* 33:2465–2482
- Qiu B, Chen S (2005) Variability of the Kuroshio extension jet, recirculation gyre and mesoscale eddies on decadal timescales. *J Phys Oceanogr* 35:2090–2103
- Qiu B, Chen S (2010) Eddy-mean flow interaction in the decadal-modulating Kuroshio extension system. *Deep-Sea Res II* 57:1097–1110. <https://doi.org/10.1016/j.dsr2.2008.11.036>
- Sasaki YN, Minobe S, Schneider N (2013) Decadal response of the Kuroshio extension jet to Rossby waves: observation and thin-jet theory\*. *J Phys Oceanography* 43:442–456. <https://doi.org/10.1175/JPO-D-12-096.1>
- Sérazin G, Jaymond A, Leroux S, Penduff T, Bessières L, Llovel W, Barnier B, Molines J-M, Terray L (2017) A global probabilistic study of the ocean heat content low-frequency variability: atmospheric forcing versus oceanic chaos: forced and chaotic OHC variability. *Geophys Res Lett*. <https://doi.org/10.1002/2017GL073026>
- Stainforth D, Allen M, Tredger ER, Smith LA (2007) Confidence, uncertainty and decision-support relevance in climate predictions. *Phil Trans R Soc* 365:2145–2161. <https://doi.org/10.1098/rsta.2007.2074>
- Sushama L, Ghil M, Ide K (2007) Spatio-temporal variability in a mid-latitude ocean basin subject to periodic wind forcing. *Atmos Ocean* 45(4):227–250. <https://doi.org/10.3137/ao.450404>
- Taylor KE (2001) Summarizing multiple aspects of model performance in a single diagram. *J Geophys Res* 106:7183–7192. <https://doi.org/10.1029/2000JD900719>
- Taguchi B, Xie S-P, Schneider N, Nonaka M, Sasaki H, Sasai Y (2007) Decadal variability of the Kuroshio extension: observations and an eddy-resolving model hindcast. *J Clim* 20:2357–2377
- Wang Y, Yang X, Hu J (2016) Position variability of the Kuroshio extension sea surface temperature front. *J Acta Oceanol Sin* 35:30. <https://doi.org/10.1007/s13131-016-0909-7>
- Wyrtki K, Magaard L, Hagar J (1976) Eddy energy in the oceans. *J Geophys Res* 81:2641–2646
- Yang Y, Liang XS (2016) The instabilities and multiscale energetics underlying the mean–interannual–eddy interactions in the Kuroshio extension region. *J Phys Oceanogr* 46:1477–1494. <https://doi.org/10.1175/JPO-D-15-0226.1>
- Zhang J, Luo DH (2017) Impact of Kuroshio extension dipole mode variability on the North Pacific storm track. *Atmos Ocean Sci Lett* 10(5):389–396. <https://doi.org/10.1080/16742834.2017.1351864>

**Publisher's Note** Springer Nature remains neutral with regard to jurisdictional claims in published maps and institutional affiliations.